Vortex Models for Feedback Stabilization of Wake Flows

Bartosz Protas

Department of Mathematics & Statistics, McMaster University, Hamilton, Ontario, Canada,
bprotas@mcmaster.ca,
WWW home page: http://www.math.mcmaster.ca/bprotas

Summary

This paper reviews recent progress concerning development of point–vortex reduced–order models for feedback stabilization of the cylinder wake flow. First, we recall briefly some earlier results related to the design of linear feedback stabilization strategies based on the Föppl system. Then we present derivation of a higher–order Föppl system based on solutions of the Euler equations which desingularize the original Föppl vortices. We argue that such higher–order Föppl systems possess important advantages over the classical Föppl system which are relevant from the control–theoretic point of view. In particular, we present computational results indicating that a higher–order Föppl system can be stabilized completely in contrast to the classical Föppl system for which this is not possible owing to the presence of a stable center manifold spanned by uncontrollable modes.

1 Introduction

The Navier–Stokes equations and most of their simplified versions such as, for instance, the Euler equations, are infinite–dimensional dynamical systems and therefore their solutions are characterized by an infinite number of parameters. Despite the fact that the infinite–dimensional Control Theory is well developed, most of the readily available computational control algorithms have finite–dimensional systems as their point of departure. This justifies the need for deriving finite–dimensional representations of the steady solutions that one intends to stabilize and deriving finite–dimensional descriptions of the system dynamics in the neighborhood of such unstable solutions, the so–called "reduced–order models". As regards derivation of such finite–dimensional representations, there are two main approaches which can be roughly classified as "data–based" and "equation–based". The approaches belonging to the first family rely on finding empirical basis functions which optimally span, in some suitable sense, the data characterizing the system and collected during its evolution. The best known approach in this category is the Proper Orthogonal Decomposition (POD) whose application for flow control purposes was reviewed by [1]. Application of such data–based approaches to development of reduced–order models is however limited to regimes well–represented by the data available. Such models may therefore provide rather poor representation of the system response

to arbitrary forcing, as it may push the system trajectories towards regimes not described by the available empirical data. On the other hand, equation–based approaches seek to construct finite–dimensional representations as solutions of truncated finite–dimensional forms of the governing equations. The most common approaches belonging to this category use standard space discretizations of the original partial differential equations to generate finite–dimensional models of the system. Examples of flow control techniques developed based on such models are described, for instance, by [2] and [3]. In the present investigation we will pursue an alternative approach where we will consider simplified forms of the governing equations which, while remaining infinite–dimensional, are easier to solve and analyze. Solutions of such simplified equations can be treated using analytical techniques, so that suitable truncation of the obtained expressions will lead to the reduced–order models. The present paper is concerned with development of a systematic procedure for generation of such reduced–order models of certain hydrodynamic systems.

We are interested here in constructing simple reduced–order models for vortex–dominated flows, hence we will assume that the flow is incompressible and inviscid. Therefore, instead of solutions of the Navier–Stokes equations, we will consider solutions of the Euler equations. It is well–known [4] that 2D steady–state Euler equations can be equivalently represented as

$$\begin{cases} \Delta\psi = f(\psi) & \text{in } \Omega, \\ \psi = 0 & \text{on } \partial\Omega, \\ \psi \to U_\infty y & \text{for } |(x,y)| \to \infty, \end{cases} \tag{1}$$

where ψ is the streamfunction, which allows the velocity components to be expressed as $u = \frac{\partial\psi}{\partial y}$ and $v = -\frac{\partial\psi}{\partial x}$, and f is an arbitrary function representing the relationship between the streamfunction and the vorticity ω as $\omega = f(\psi)$. In this investigation we are interested only in solutions symmetric with respect to the flow centerline, so without loss of generality we can restrict Ω in (1) to the upper half–plane (i.e., points with $y > 0$). We note that the indeterminacy of the function f in (1) reflects the nonuniqueness of solutions of the Euler equations in a given domain Ω. For instance, expressing the function $f(\psi)$ on the RHS as a linear combination of $2K$ Dirac delta distributions $\sum_{k=1}^{2K} \Gamma_k \delta(x - x_k)\delta(y - y_k)$ with weights Γ_k, where K is the total number of singularities and their images, leads to systems known from the classical potential flow theory corresponding to $2K$ point vortices located at the points $\{x_k, y_k\}_{k=1}^{2K}$. An example of such a solution was found in closed form by Föppl in [5], where the potential flow was obtained by placing behind the obstacle two counter–rotating point vortices located symmetrically with respect to the centerline (Figure 1a). With points of the plane characterized by their complex coordinates $z = x + iy$, where $i = \sqrt{-1}$, the complex potential of this flow $W_0(z) = (\varphi + i\psi)(z)$, where φ and ψ are, respectively, the potential and the streamfunction, can be expressed as

$$W_0(z) = W_C(z) + W_{F,0}(z), \tag{2}$$

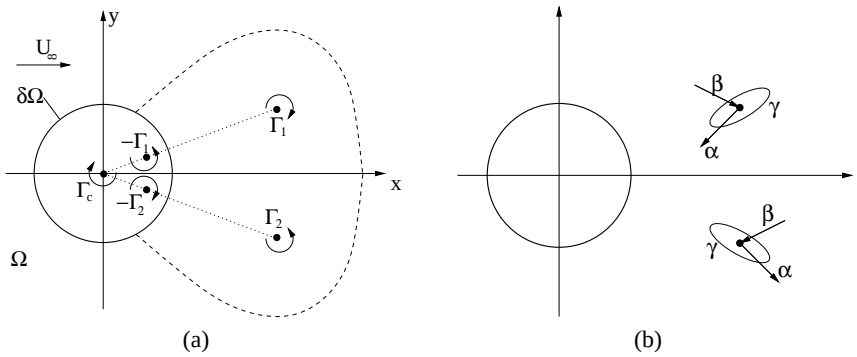

Figure 1 Schematics showing (a) the location of the singularities in the classical Föppl system and (b) the three modes of motion characterizing the linearized Föppl system (7): the unstable mode α, the asymptotically stable mode β and the neutrally stable (oscillatory) mode γ. In Figure (a) the dashed line represents the separatrix streamline delimiting the recirculation region.

where

$$W_C(z) = U_\infty \left(z + \frac{R^2}{z} \right), \tag{2a}$$

$$W_{F,0}(z) = \frac{\Gamma_0}{2\pi i} \left[\ln(z - z_0) - \ln\left(z - \frac{R^2}{\overline{z}_0} \right) - \ln(z - \overline{z}_0) + \ln\left(z - \frac{R^2}{z_0} \right) \right] \tag{2b}$$

and Γ_0 and $z_0 = x_0 + iy_0$ represent, respectively, the circulation and position of the Föppl vortices. In Equation (2) $W_C(z)$ represents the base flow symmetric with respect to the OY axis and due to the cylinder only, whereas $W_{F,0}(z)$ corresponds to the two Föppl vortices located at z_0 and $\overline{z}_0$ and their two images located inside the obstacle. Two one–parameter families of steady vortex configurations given by (2) were found by Föppl in [5]: the configuration characterized by the condition

$$\begin{cases} (|z_0|^2 - R^2)^2 = 4|z_0|^2 y_0^2, \\ \Gamma_0 = -2\pi \dfrac{(|z_0|^2 - R^2)^2 (|z_0|^2 + R^2)}{|z_0|^5}, \end{cases} \tag{3}$$

hereafter referred to as the "classical Föppl system" (Figure 1a), and the configuration characterized by the condition $\Re(z_0) = 0$, i.e., corresponding to the vortices located on the OY axis. The latter solution, however, does not correspond to any physical situation and will not be discussed further in this investigation.

The classical Föppl system has recently been used as a reduced–order model in the development of a simple feedback stabilization strategy for the cylinder wake flow in [6]. The cylinder rotation $\Gamma_C = \Gamma_C(t)$ was used the flow actuation (i.e., the control variable) and observations of the centerline velocity downstream of the obstacle as the system output. The advantage of this approach is that, due to simplicity

of the Föppl model, the synthesis of the stabilization algorithm becomes a simple task with a significant part of the calculations carried out analytically. The performance of the stabilization strategy, while quite encouraging, also showed some limitations of such very simple point–vortex systems employed as reduced–order models. The purpose of this investigation is to identify sources of these limitations and propose possible improvements. The structure of the paper is as follows: first in Section 2 we review the formulation of the Linear–Quadratic–Gaussian (LQG) compensator designed based on the Föppl system as a reduced–order model, in Section 3 we introduce a family of higher–order Föppl systems characterized by more desirable properties as candidates for reduced–order models, then some computational results are presented in Section 4 and conclusions are deferred to Section 5.

2 Control Design Based on the Föppl System as a Reduced–Order Model

We begin this Section by analyzing the stability properties of the classical Föppl system linearized around the equilibrium solution. This analysis will motivate the design of an LQG compensator for feedback stabilization of the linearized Föppl system. Careful analysis of the linear stability of the Föppl system and its relevance to modeling the onset of vortex shedding in 2D wake flows was presented by Tang and Aubry in [7]. Our discussion of the control–theoretic aspects will be here necessarily concise and the reader is referred to the publication [6] for further details. Different flow control problems also based on the Föppl system as the reduced–order model were studied in [8, 9].

We will assume that the cylinder has unit radius $R = 1$ and the free stream at infinity has unit magnitude $U_\infty = 1$. In addition, we will also assume that all quantities are nondimensionalized using these values. The Föppl model can be regarded as a nonlinear dynamical system with evolution described by

$$\frac{d}{dt}\mathbf{X} = \mathbf{F}(\mathbf{X}) + \mathbf{b}(\mathbf{X})\Gamma_C \triangleq \begin{bmatrix} \Re[V_1(z_1, z_2, \Gamma_1, \Gamma_2)] \\ -\Im[V_1(z_1, z_2, \Gamma_1, \Gamma_2)] \\ \Re[V_2(z_1, z_2, \Gamma_1, \Gamma_2)] \\ -\Im[V_2(z_1, z_2, \Gamma_1, \Gamma_2)] \end{bmatrix} + \mathbf{b}(\mathbf{X})\Gamma_C, \tag{4}$$

where $\mathbf{X} \triangleq [x_1 \;\; y_1 \;\; x_2 \;\; y_2]^T$ is the state vector and the control matrix $\mathbf{b}(\mathbf{X})$ is expressed as

$$\mathbf{b}(\mathbf{X}) \triangleq \frac{1}{2\pi} \begin{bmatrix} -y_1/|z_1|^2 \\ x_1/|z_1|^2 \\ y_2/|z_2|^2 \\ x_2/|z_2|^2 \end{bmatrix}. \tag{5}$$

The expressions for V_1 and V_2 in (4) are given by the velocity field

$$\begin{aligned} V(z) = 1 - \frac{1}{z^2} - \frac{\Gamma_1}{2\pi i}\left(\frac{1}{z - z_1} - \frac{1}{z - 1/\overline{z}_1}\right) \\ + \frac{\Gamma_2}{2\pi i}\left(\frac{1}{z - z_2} - \frac{1}{z - 1/\overline{z}_2}\right) + \frac{\Gamma_C}{2\pi i z}, \end{aligned} \tag{6}$$

evaluated at z_1 and z_2 with the singular "self–induction" terms ($\frac{1}{z-z_1}$ and $\frac{1}{z-z_2}$, respectively) omitted. For the moment we will fix attention on the properties of the Föppl system without control, hence we will assume that $\Gamma_C \equiv 0$, which renders (4) autonomous.

The linear stability analysis of the Föppl system is performed by adding the perturbations (x_1', y_1') and (x_2', y_2') to the coordinates of the upper and lower vortex of the stationary solution and then linearizing the system (4) around $\mathbf{X}_0 \triangleq [x_0 \;\; y_0 \;\; x_0 \;\; -y_0]^T$ assuming small perturbations. Thus, evolution of the perturbations is governed by the system

$$\frac{d}{dt}\mathbf{X}' = \mathbf{A}\mathbf{X}', \tag{7}$$

where $\mathbf{X}' \triangleq [x_1' \;\; y_1' \;\; x_2' \;\; y_2']^T$ is the perturbation vector and the system matrix is given by the Jacobian of the nonlinear system at the equilibrium $\mathbf{A} = \frac{\partial \mathbf{F}}{\partial \mathbf{X}}(\mathbf{X}_0)$. We remark that (7) is a linear time–invariant (LTI) system. Eigenvalue analysis of the matrix $\mathbf{A}$ reveals (see [7] for details) the presence of the following modes of motion (Figure 1b):

- unstable (growing) mode α corresponding to a positive real eigenvalue $\lambda_1 = \lambda_r > 0$,
- stable (decaying) mode β corresponding to a negative real eigenvalue $\lambda_2 = -\lambda_r < 0$,
- neutrally stable oscillatory mode γ corresponding to a conjugate pair of purely imaginary eigenvalues $\lambda_{3/4} = \pm i\lambda_i$.

These qualitative properties are independent of the downstream coordinate x_0 characterizing the equilibrium solution. The analysis of the orientation of the unstable eigenvectors carried out in [7] revealed that the initial stages of instability of the Föppl system closely resemble the onset of vortex shedding in an actual cylinder wake undergoing Hopf bifurcation. The free parameter characterizing the equilibrium solution (3) of the Föppl system (i.e., the downstream location of the singularities x_0) is chosen here, so that the length of the recirculation zone in the Föppl system is the same as the recirculation length in the steady unstable solution of the Navier–Stokes system at a prescribed Reynolds number. Further justification as well as details of calculations are described in [6]. In the examples presented hereafter the downstream position of the vortices was chosen, so that the recirculation length is the same as in the steady unstable solution of the Navier–Stokes system at the Reynolds number $Re = 75$.

After including the control term representing the cylinder rotation the linearized Föppl system becomes

$$\frac{d}{dt}\mathbf{X}' = \mathbf{A}\mathbf{X}' + \mathbf{B}\Gamma_C, \tag{8}$$

where

$$\mathbf{B} \triangleq \mathbf{b}(\mathbf{X}_0) = \frac{1}{2\pi r_0^2}\begin{bmatrix} -y_0 \\ x_0 \\ y_0 \\ x_0 \end{bmatrix}. \tag{9}$$

As mentioned in Section 1 our control objective is attenuation of vortex shedding which can be quantified by measuring the velocity at a point on the flow centerline with the streamwise coordinate x_m (note that in the stationary symmetric solution the transverse velocity component vanishes on the centerline). Choosing this quantity as an output of system (4) we obtain the following output equation

$$\mathbf{h}(z_1,z_2) \triangleq \begin{bmatrix} \Re[V(x_m)] \\ -\Im[V(x_m)] \end{bmatrix} + \mathbf{D}\Gamma_C, \tag{10}$$

where the matrix $\mathbf{D} \triangleq \frac{1}{2\pi x_m^2}[0 \; x_m]^T$ represents the control–to–measurements map. Linearization of equation (10) yields

$$\mathbf{h}(z_0+z_1',\overline{z}_0+z_2') \cong \mathbf{h}(z_0,\overline{z}_0) + \mathbf{C}\mathbf{X}', \tag{11}$$

where $z_k' = x_k' + iy_k'$, $k = 1,2$, and the linearized observation operator $\mathbf{C}$ is given by

$$\mathbf{C} = \begin{bmatrix} \frac{\partial u(x_m)}{\partial x_1}\Big|_{(x_0,y_0)} & \frac{\partial u(x_m)}{\partial y_1}\Big|_{(x_0,y_0)} & \frac{\partial u(x_m)}{\partial x_2}\Big|_{(x_0,y_0)} & \frac{\partial u(x_m)}{\partial y_2}\Big|_{(x_0,y_0)} \\ \frac{\partial v(x_m)}{\partial x_1}\Big|_{(x_0,y_0)} & \frac{\partial v(x_m)}{\partial y_1}\Big|_{(x_0,y_0)} & \frac{\partial v(x_m)}{\partial x_2}\Big|_{(x_0,y_0)} & \frac{\partial v(x_m)}{\partial y_2}\Big|_{(x_0,y_0)} \end{bmatrix}. \tag{12}$$

Uncertainty of the reduced–order model is represented by the presence of noise w which affects the linearized system dynamics via a $[4\times 1]$ matrix $\mathbf{G}$ and the linearized system output via a $[2\times 1]$ matrix $\mathbf{H}$. Moreover, we assume that the velocity measurements may be additionally contaminated with noise $\mathbf{m} \triangleq [m_1 \; m_2]^T$, where m_1 and m_2 are stochastic processes. With these definitions we can now put the linearized reduced–order model in the standard state–space form (see [10])

$$\frac{d}{dt}\mathbf{X}' = \mathbf{A}\mathbf{X}' + \mathbf{B}\Gamma_C + \mathbf{G}w, \tag{13a}$$

$$\mathbf{Y} = \mathbf{C}\mathbf{X}' + \mathbf{D}\Gamma_C + \mathbf{H}w + \mathbf{m}. \tag{13b}$$

Prior to designing a controller for system (13) we have to verify whether the system is controllable and observable which is done by studying the ranks $\mathcal{N}_c$ and $\mathcal{N}_o$ of the controllability and observability Grammians

$$\mathcal{N}_c \triangleq \operatorname{rank}\left[\mathbf{B} \;\; \mathbf{A}\mathbf{B} \;\; \mathbf{A}^2\mathbf{B} \;\; \mathbf{A}^3\mathbf{B}\right] = 2, \tag{14}$$

$$\mathcal{N}_o \triangleq \operatorname{rank}\left[\mathbf{C}^T \;\; \mathbf{A}^T\mathbf{C}^T \;\; (\mathbf{A}^T)^2\mathbf{C}^T \;\; (\mathbf{A}^T)^3\mathbf{C}^T\right] = 4. \tag{15}$$

We conclude that the matrix pair $\{\mathbf{A},\mathbf{B}\}$ is not controllable and only two out of four modes present in the system can be controlled. On the other hand, the matrix pair $\{\mathbf{A},\mathbf{C}\}$ is completely observable. Converting system (13) to the minimal representation which consists of those modes only which are both controllable and observable will allow us to determine which modes are in fact controllable. We accomplish this by introducing an orthogonal transformation matrix

$$\mathbf{T}_c \triangleq \sqrt{2}\begin{bmatrix} 1/2 & 0 & -1/2 & 0 \\ 0 & 1/2 & 0 & 1/2 \\ 1/2 & 0 & 1/2 & 0 \\ 0 & 1/2 & 0 & -1/2 \end{bmatrix} \tag{16}$$

and making the following change of variables $\mathbf{X}'_{ab} \triangleq \begin{bmatrix}\mathbf{X}'_a \\ \mathbf{X}'_b\end{bmatrix} = \mathbf{T}_c\mathbf{X}'$. The corresponding form of system (13) is now

$$\frac{d}{dt}\begin{bmatrix}\mathbf{X}'_a \\ \mathbf{X}'_b\end{bmatrix} = \begin{bmatrix}\mathbf{A}_a & \mathbf{0} \\ \mathbf{0} & \mathbf{A}_b\end{bmatrix}\begin{bmatrix}\mathbf{X}'_a \\ \mathbf{X}'_b\end{bmatrix} + \begin{bmatrix}\mathbf{B}_a \\ \mathbf{0}\end{bmatrix}\Gamma_C + \begin{bmatrix}\mathbf{G}_a \\ \mathbf{G}_b\end{bmatrix} w, \tag{17a}$$

$$\begin{bmatrix}Y_b \\ Y_a\end{bmatrix} = \begin{bmatrix}\mathbf{0} & \mathbf{C}_b \\ \mathbf{C}_a & \mathbf{0}\end{bmatrix}\begin{bmatrix}\mathbf{X}'_a \\ \mathbf{X}'_b\end{bmatrix} + \begin{bmatrix}D_1 \\ D_2\end{bmatrix}\Gamma_C + \begin{bmatrix}H_1 \\ H_2\end{bmatrix} w + \mathbf{m}. \tag{17b}$$

Our minimal representation is thus given by the upper row in equation (17a) and the lower row in (17b), i.e.,

$$\frac{d}{dt}\mathbf{X}'_a = \mathbf{A}_a\mathbf{X}'_a + \mathbf{B}_a\Gamma_C + \mathbf{G}_a w, \tag{18a}$$

$$Y_a = \mathbf{C}_a\mathbf{X}'_a + D_2\Gamma_C + H_2 w + m_2. \tag{18b}$$

Eigenvalue analysis of the matrices $\mathbf{A}_a$ and $\mathbf{A}_b$ reveals that $\mathbf{A}_a$ has two real eigenvalues (positive and negative) corresponding to the growing and decaying modes α and β, whereas the matrix $\mathbf{A}_b$ has a conjugate pair of purely imaginary eigenvalues which correspond to the neurally stable mode γ (Figure 1b). Hence, the uncontrollable part of the model system dynamics is associated with the neutrally stable oscillatory mode γ and the original system (13) is thus *stabilizable*, but not *controllable*. Practical effectiveness of the proposed algorithm depends on the location of the velocity sensor x_m. As argued in [6], the distance x_m is chosen so as to maximize the observability residual of the unstable mode α.

Our objective here is to find a *feedback* control law $\Gamma_C = -\mathbf{K}\mathbf{X}'$, where $\mathbf{K}$ is a $[4 \times 1]$ feedback matrix, that will

1. stabilize system (13) and
2. minimizing a performance criterion represented by the following cost functional

$$\mathcal{J}(\Gamma_C) \triangleq E\left[\int_0^\infty (\mathbf{Y}^T\mathbf{Q}\mathbf{Y} + \Gamma_C R\Gamma_C)dt\right], \tag{19}$$

where E denotes the expectation, $\mathbf{Q}$ is a symmetric positive semi–definite matrix and $R > 0$.

Note that the cost functional (19) represents a sum of the linearized system output $\mathbf{Y}$ [i.e., the velocity at the sensor location $(x_m, 0)$] and the control effort. The feedback control law determines the actuation (i.e., the circulation of the control vortex Γ_C representing the cylinder rotation) based on the state of the reduced–order model (i.e., the perturbation $\mathbf{X}'$ of the stationary solution). In practice, however, the state $\mathbf{X}'$ of the model (13) is not known. Instead, noisy measurements $\tilde{\mathbf{Y}} = [\tilde{Y}_b \;\; \tilde{Y}_a]^T$ of the actual system [i.e., the nonlinear Föppl model (4) or an actual wake flow] are available and can be used in an *estimation procedure* to construct an estimate $\mathbf{X}'_e$ of the model state $\mathbf{X}'$. The evolution of the state estimate $\mathbf{X}'_e$ is governed by the

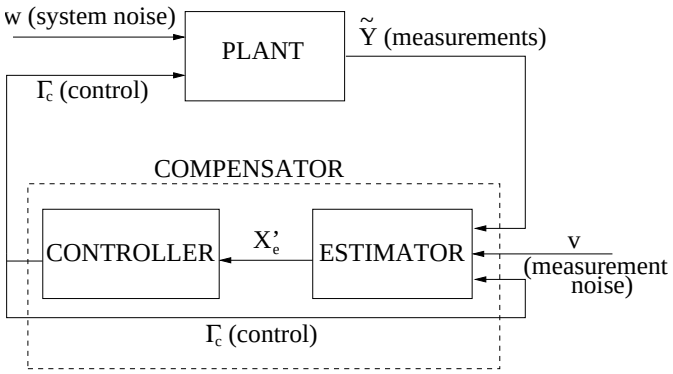

Figure 2 Schematic of a compensator composed of an estimator and a controller.

estimator system

$$\frac{d}{dt}\mathbf{X}'_e = \mathbf{A}\mathbf{X}'_e + \mathbf{B}\boldsymbol{\Gamma}_C + \mathbf{L}(\tilde{\mathbf{Y}} - \mathbf{Y}_e), \tag{20a}$$

$$\mathbf{Y}_e = \mathbf{C}\mathbf{X}'_e + \mathbf{D}\boldsymbol{\Gamma}_C, \tag{20b}$$

where $\mathbf{L}$ is a feedback matrix that can be chosen in a manner ensuring that the estimation error vanishes in the infinite time horizon, i.e., that $\mathbf{X}'_e \to \mathbf{X}'$ as $t \to \infty$. Thus, the estimator assimilates available observations into the system model, so as to produce an evolving estimate of the system state. Finally, the controller and the estimator can be combined to form a compensator in which the feedback control is determined based on the state estimate $\mathbf{X}'_e$ as

$$\boldsymbol{\Gamma}_C = -\mathbf{K}\mathbf{X}'_e. \tag{21}$$

The flow of information in a compensator is shown schematically in Figure 2. The design of a Linear–Quadratic–Gaussian (LQG) compensator can be accomplished using standard methods of Linear Control Theory (see, e.g., [10]). Here we only remark that, since system (8) is stabilizable, but not controllable, the controller can in fact be designed based on the minimal representation. On the other hand, since system (8) is observable, the estimator is designed based on the original representation. Given small dimensions of systems (7) and (18), solution of the Riccati equations at the heart of these problems does not pose any difficulties. The reader is referred to [6] for further details.

3 Higher–Order Föppl Systems

In this Section we describe potential flow solutions generalizing Föppl's classical point–vortex system. They can approximate with desired accuracy the velocity field

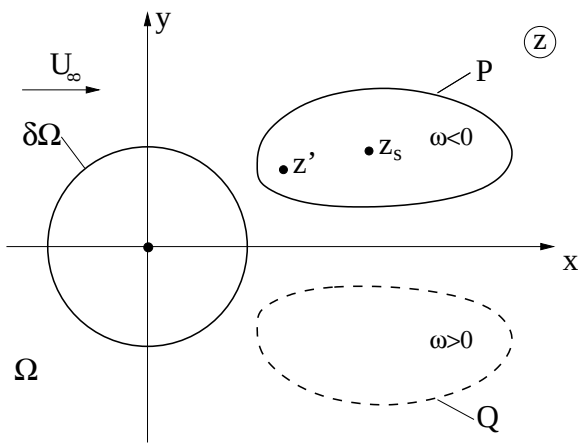

Figure 3 Schematic showing EFHM solutions with two opposite–sign vortex patches *P* (solid line) and *Q* (dashed line) located symmetrically with respect to the flow centerline.

of the steady–state solutions of the Euler equations characterized by arbitrary compact vorticity support. Such system have the same dimension as the original Föppl model, however, are characterized by an arbitrary number of adjustable parameters, hence are more flexible as reduced–order models. We consider again solutions of system (1), however, instead of a collection of Dirac delta functions now we allow for more general forms of the RHS function $f(\psi)$. A family of interesting solutions was computed by Elcrat et al. in [11] by choosing $f(\psi)$ as follows

$$f(\psi) = \begin{cases} -\omega, & \psi \leq \sigma, \\ 0, & \psi > \sigma, \end{cases} \tag{22}$$

where σ is an adjustable parameter. Such a vorticity distribution is sometimes referred to as the Rankine core. These solutions will play an important role in our development and we will hereafter refer to them as the "EFHM flows". When $\sigma < 0$, such flows are characterized by compact regions of constant vorticity embedded in an otherwise irrotational flow and are therefore related to the so–called Sadovskii flows [12]. In addition to this solution, shown schematically in Figure 3, it was found in [11] that regions of opposite–sign vorticity, hereafter denoted *P* and *Q*, may also exist above and below the obstacle, as well as in front of it. Since these solutions do not correspond to any physical situation, they will not be considered hereafter.

Consider a compact region *P* of vorticity embedded in an irrotational flow past a circular cylinder (Figure 3) and characterized by the vorticity distribution $\omega = \omega(z)$. When $\omega = Const$, the corresponding steady–state solutions of the Euler equations defined by (1) and (22) are given by families of the EFHM flows computed in [11]. Below we construct algebraic systems that are approximations of such solutions. Our approach is conceptually related to the method devised by [13] in which mo-

ments of vorticity distribution are used to characterize the evolution of a system of vortex patches. Using complex Green's function for the Laplace equation in a 2D unbounded domain $G(z,z') = \frac{1}{2\pi i}\ln(z-z')$, the complex potential induced by a vortex patch in such a domain can be expressed for points outside the patch $z \notin P$ as

$$\tilde{W}_P(z) = (\varphi + i\psi)(z) = \frac{1}{2\pi i}\int_P \ln(z-z')\omega(z')\,dA(z'), \tag{23}$$

where $dA(z') = dx'dy'$. Tilde ($\tilde{}$) indicates that this potential represents a flow in an unbounded domain (i.e., without the obstacle), whereas the subscript indicates that the potential is due to the patch P. We now choose a point $z_s \in P$ as the origin of the local coordinate system associated with the patch P and set $\zeta = z' - z_s$ (see Figure 3). The complex potential (23) can now be expressed as

$$\tilde{W}_P(z) = \frac{\Gamma_0}{2\pi i}\ln(z-z_s) + \frac{1}{2\pi i}\int_P \ln\left(1 - \frac{\zeta}{z-z_s}\right)\omega(z_s+\zeta)\,dA(\zeta). \tag{24}$$

The second term in (24) can, for $|z-z_s| > |z'-z_s|$, be expanded in a Taylor series which yields

$$\tilde{W}_P(z) = \frac{\Gamma_0}{2\pi i}\ln(z-z_s) - \frac{1}{2\pi i}\sum_{n=1}^{\infty}\frac{c_n}{n}(z-z_s)^{-n}, \quad |z-z_s| > \zeta_m, \tag{25}$$

where

$$c_n(z_s) = \int_P \omega(z_s+\zeta)\zeta^n\,dA(\zeta) \tag{26}$$

and $\zeta_m = \max_{(z_s+\zeta)\in P}|\zeta|$. Thus, the point z_s represents also the location of a singularity which, for the moment, remains unspecified. The quantities $c_n(z_s)$, $n = 1,\ldots,N$ are the moments of the vorticity distribution in the patch P with respect to the point z_s and therefore are related to the eccentricity of the patch (c_1), its ellipticity (c_2), etc. (unless required for clarity, hereafter we will skip the argument of c_n). The zeroth moment c_0 is equal to the total circulation Γ_0 of the patch. The complex potential due to a finite–area vortex patch P can be approximated for points of the plane lying outside this patch by truncating expression (25), i.e., replacing it with a finite sum of singularities located at the point z_s

$$\tilde{W}_P(z) \cong \tilde{W}_{P,N}(z) = \frac{\Gamma_0}{2\pi i}\ln(z-z_s) - \frac{1}{2\pi i}\sum_{n=1}^{N}\frac{c_n}{n}(z-z_s)^{-n}, \quad |z-z_s| > \zeta_m. \tag{27}$$

The order of truncation is represented by the second subscript on $\tilde{W}$. The complex potential $\tilde{W}_{Q,N}(z)$ due to the patch Q with the opposite–sign vorticity and located symmetrically below the flow centerline (Figure 3) can be represented using an analogous expression in which z_s is replaced with $\overline{z}_s$ and c_n with $-\overline{c}_n$ for $n = 1,\ldots,N$. Below we use these expressions to construct potential flows approximating solutions of the steady–state Euler equations (1) in the sense that the velocity field of the potential flow will converge, for $z \notin P$ and $z \notin Q$, to the velocity field of the Euler

flow as $N \to \infty$. These potential flows are constructed using the potentials $\tilde{W}_{P,N}(z)$ and $\tilde{W}_{Q,N}(z)$, and adding suitable "image singularities" located inside the obstacle in a way ensuring that the boundary conditions for the wall–normal velocity component are satisfied. In general, such flows can be constructed using the "Circle Theorem" [4] which states that if $\tilde{w}(z)$ is the complex potential of a flow in an unbounded domain and with singularities at some points z_k, such that $\forall k,\ |z_k| > R$, then the complex potential of the corresponding flow past the cylinder with radius R is given by the expression $w(z) = \tilde{w}(z) + \overline{\tilde{w}}(\frac{R^2}{z})$. Thus, using this construction to enforce the boundary conditions and including also the base flow with the potential $W_C(z)$ [cf. Eq. (2)], we obtain the following expression for the complex potential

$$
\begin{aligned}
W_N(z) &= W_C(z) + W_{F,N}(z) \\
&= W_C(z) + \tilde{W}_{P,N}(z) + \tilde{W}_{Q,N}(z) + \overline{\tilde{W}}_{P,N}\left(\frac{R^2}{z}\right) + \overline{\tilde{W}}_{Q,N}\left(\frac{R^2}{z}\right) \\
&= U_\infty\left(z + \frac{R^2}{z}\right) - \frac{\Gamma_0}{2\pi i}\left[\ln(z - z_s) - \ln\left(z - \frac{R^2}{\overline{z}_s}\right) - \right. \\
&\quad \left. \ln(z - \overline{z}_s) + \ln\left(z - \frac{R^2}{z_s}\right)\right] - \frac{1}{2\pi i}\sum_{n=1}^{N}\frac{1}{n}\left[\frac{c_n}{(z - z_s)^n}\right. \\
&\quad \left. - (-1)^n \frac{\overline{c}_n}{\left(z - \frac{R^2}{\overline{z}_s}\right)^n}\left(\frac{z}{\overline{z}_s}\right)^n - \frac{\overline{c}_n}{(z - \overline{z}_s)^n} + (-1)^n \frac{c_n}{\left(z - \frac{R^2}{z_s}\right)^n}\left(\frac{z}{z_s}\right)^n\right],
\end{aligned}
\tag{28}
$$

where $W_{F,N}(z)$ represents the truncated potential due to the finite–area vortex patches and their images. We notice that setting $N = 0$ in (28) we recover the complex potential (2) of the classical Föppl system discussed in Section 1. Therefore, the family of the complex potentials given in (28) represents N–th order corrections to the Föppl system regarded as approximations of the corresponding solution of the steady–state Euler equations and hereafter we will refer to them as the "higher–order (N–th order) Föppl systems". By taking N large enough we can obtain an arbitrarily accurate representation of the velocity field in the Euler flow valid for points in the flow domain outside the vortex patches, thereby improving applicability of the Föppl system as a model for steady wake flows.

In general, in an inviscid and incompressible fluid singularities (e.g., a point vortex located at z_s) move according to the velocity field $\frac{d\overline{z}_s}{dt} = \hat{V}_N(z_s)$, where complex conjugation is required to account for the fact that the complex velocity field is given by $\hat{V}_N = \hat{u} - i\hat{v}$. We note that the advection velocity $\hat{V}_N$ of a singularity is not affected by its self–induction which can be seen by regarding the singularity as a limit of a sequence of finite–area circular distributions of the corresponding quantity. The velocity induced by such distributions can be shown to vanish at their center. Thus, the advection velocity of a singularity is obtained as

$$
\hat{V}_N(z) = V_N(z) - \frac{1}{2\pi i}\left[-\frac{\Gamma_0}{z - z_s} + \sum_{n=1}^{N}\frac{c_n}{(z - z_s)^{n+1}}\right], \tag{29}
$$

where $V_N(z) = \frac{dW_N(z)}{dz}$, i.e., the terms which become singular as $z \to z_s$ are removed from the velocity field. Hereafter, hats ($\hat{}$) will distinguish quantities with these self–inductions terms subtracted off. We are interested in steady–state solutions of the higher–order Föppl systems, therefore, for a given truncation order N, we need to find the equilibrium points of system (29), i.e., the points z_N such that setting $z_s = z_N$ the following condition is satisfied for given Γ_0 and $\{c_n\}_{n=1}^N$

$$\hat{V}_N(z_N) = 0. \tag{30}$$

This condition can be expanded to

$$\begin{aligned}\hat{V}_N(z_N) = U_\infty \left(1 - \frac{R^2}{z_N^2}\right) - \frac{\Gamma_0}{2\pi i}\left[-\frac{1}{\left(z_N - \frac{R^2}{\overline{z}_N}\right)} - \frac{1}{(z_N - \overline{z}_N)} + \frac{1}{\left(z_N - \frac{R^2}{z_N}\right)}\right] \\ + \frac{1}{2\pi i}\sum_{n=1}^{N}\left[(-1)^{n+1}\frac{R^2\overline{c}_n}{\left(z_N - \frac{R^2}{\overline{z}_N}\right)^{n+1}}\frac{z_N^{n-1}}{\overline{z}_N^{n+1}}\right. \\ \left. - \frac{\overline{c}_n}{(z_N - \overline{z}_N)^{n+1}} - (-1)^{n+1}\frac{R^2 c_n}{\left(z_N - \frac{R^2}{z_N}\right)^{n+1}}\frac{1}{z_N^2}\right] = 0\end{aligned} \tag{31}$$

which is a complex–valued equation characterizing one complex unknown z_N. In the case when $N = 0$, one solution of (31) is given by (3). When $N \geq 1$, solutions must be found numerically, e.g. using Newton's method. Furthermore, since the order of the equation increases with N, it can be anticipated that so does the number of roots. In fact, it can be proved that there is always one root of (31) that is in a neighborhood of the solution characterized by (3) and the size of this neighborhood can be bounded by the magnitudes of the coefficients c_n. Thorough analysis of this and other analytical properties of the higher–order Föppl system is deferred to a forthcoming paper [14].

4 Computational Results

In this Section we present some preliminary computational results concerning construction of a higher–order Föppl system for a given EFHM flow and application of such a system as a reduced–order model to the design of an LQG–based stabilization strategy. Because of space limitations, our discussion here is necessarily short and the reader is referred to the forthcoming papers [14, 15] for further particulars regarding the computational procedure and detailed results. To fix attention, we will focus on the Föppl system with the singularities located at $[x_0, y_0] = [4.32, \pm 2.3596]$ and with the circulation of the vortices given by $\Gamma_0 = -29.6015$ (this is the configuration investigated in [6]). We will also consider an EFHM flow with the area of the vortex patch $A = 20.43$ as a desingularization of the classical Föppl system and

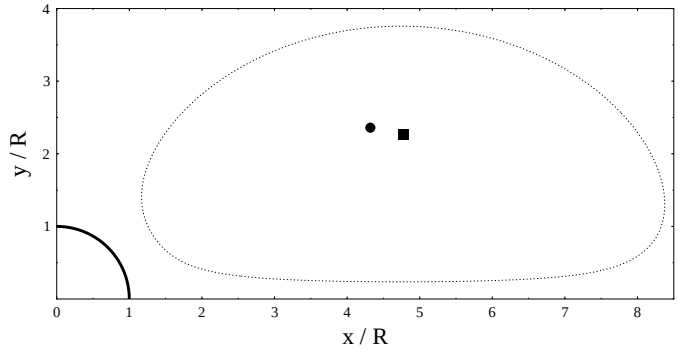

(a)

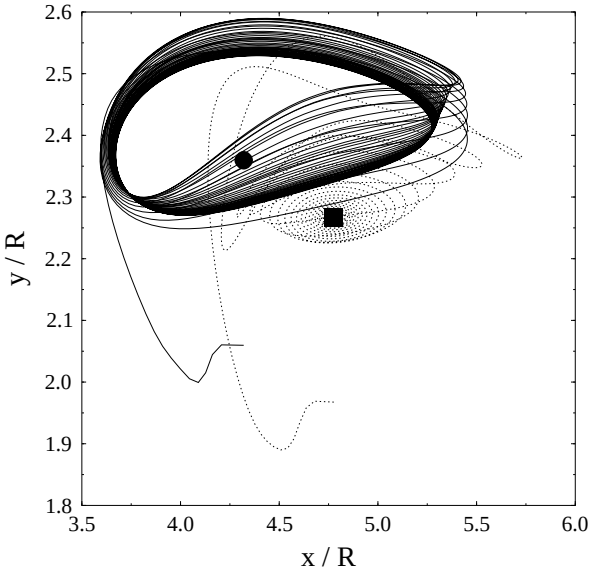

(b)

Figure 4 (a) Location of the equilibria of (circle) the classical Föppl system (3) and (square) the higher–order Föppl system (31) with $N = 10$. The boundary of the vortex patch in the EFHM flows used to construct the higher–order Föppl system is represented by the dotted line and the cylinder boundary is represented by a thick solid line. (b) Trajectories of the state of (solid line) the classical and (dotted line) higher–order Föppl system stabilized with an LQG compensator in the neighborhood of the corresponding equilibrium solutions.

will take $N = 10$ as the truncation order in the construction of the higher–order system. As analyzed in detail in [14], such higher–order systems are characterized by multiple solutions, however, in our analysis below we will focus on the equilibrium $[x_N, y_N]$ in the neighborhood of $[x_0, y_0]$, both of which are shown in Figure 4a.

As can be easily verified, the higher–order Föppl system linearized about the new equilibrium $[x_N, y_N]$ has the same properties in terms of controllability and observability as the classical Föppl system [cf. Eqns. (14) and (15)]. Assuming measurements of two velocity components on the flow centerline as the observations and the cylinder rotation as the actuation, all four modes are observable, but only two of them are controllable. Stability analysis of this higher–order Föppl system indicates that, in addition to a growing and decaying mode (corresponding to, respectively, the modes α and β, cf. Figure 1b) characterized by purely real eigenvalues, there exists also a mode characterized by pair of complex–conjugate eigenvalues (corresponding to the mode γ, cf. Figure 1b). However, in contrast to the classical Föppl system, these complex eigenvalues have negative real parts, hence the oscillatory mode in the higher–order Föppl system is in fact exponentially stable. This difference has important consequences when a linear stabilization strategy, such as LQG, is applied to the original nonlinear system. As illustrated in Figure 4b, when the LQG compensator is applied to the classical Föppl system, the state of the system does not return to the equilibrium, but lands instead on a closed orbit. One can prove rigorously using methods of dynamical systems that this orbit has in fact the structure of a center manifold and the trajectory of the system on this manifold is stable (see [15] for precise statements and proofs of these theorems). On the other hand, when the LQG compensator is applied to the higher–order Föppl system, the system trajectory returns to the equilibrium owing to the exponential stability of the uncontrollable modes.

5 Conclusions

The dynamics of both the classical and higher–order Föppl systems in the neighborhood of an equilibrium point is characterized by four degrees of freedom. However, in contrast to the classical system which has just one parameter, the higher—order systems are characterized by an arbitrary number of adjustable parameters represented by the expansion coefficients in (28). The number of these parameters is determined by the truncation order N. Therefore, by introducing a larger number of adjustable parameters, one can incorporate much more flexibility into Föppl–type models, so that, while remaining four–dimensional, they can reproduce more accurately certain properties of realistic flows. Advantages of having this additional flexibility were illustrated by the computational results presented in Section 4. We showed that the state of the classical Föppl system with an LQG stabilization converges to a center manifold, whose persistence prevents this state from reaching the equilibrium and, as a result, the amplitude of the state oscillations does not decrease. We conjecture that this is a possible reason for the oscillations of the velocity field in the near wake region occurring when this strategy was applied to stabilize an ac-

tual cylinder wake flow at $Re = 75$ (see [6]). On the other hand, the flexibility of the higher–order Föppl system investigated here made it possible to alter the stability properties of the new equilibrium in such way that the uncontrollable mode became stable. As a result, the same LQG compensation strategy was now able to stabilize completely the equilibrium. We anticipate that this additional flexibility of higher–order Föppl systems will play a role when employing these systems as reduced–order models to stabilization of actual cylinder wake flows. Verification of performance of such approaches is underway.

Acknowledgments

The author wishes to express his thanks to Profs. Alan Elcrat and Ken Miller for many interesting and helpful discussions regarding the EFHM flows and for providing him with a code to reproduce the results of the paper [11]. This research was supported by an NSERC Discovery Grant (Canada) and CNRS (France).

References

[1] J. Lumley and P. Blossey: "Control of Turbulence", Ann. Rev. Fluid Mech. **30**, 311-327, (1998).
[2] T. R. Bewley and S. Liu: "Optimal and robust control and estimation of linear paths to transition", J. Fluid Mech. **365**, 305-349, (1998).
[3] J. Kim: "Control of turbulent boundary layers", Phys. Fluids **15**, 1093-1105, (2003).
[4] L. M. Milne–Thompson: "Theoretical Hydrodynamics", MacMillan, (1955).
[5] L. Föppl: "Wirbelbewegung hinter einem Kreiscylinder", Sitzb. d. k. Bayr. Akad. d. Wiss. 1-17, (1913).
[6] B. Protas: "Linear Feedback Stabilization of Laminar Vortex Shedding Based on a Point Vortex Model", Phys. Fluids **16**, 4473-4488, 2004.
[7] S. Tang and N. Aubry: "On the symmetry breaking instability leading to vortex shedding", Phys. Fluids **9**, 2550-2561, (1997).
[8] S. Tang and N. Aubry: "Suppression of vortex shedding inspired by a low–dimensional model", J. Fluids and Struct. **14**, 443-468, (2000).
[9] F. Li and N. Aubry: "Feedback control of a flow past a cylinder via transverse motion", Phys. Fluids **15**, 2163-2176, (2003).
[10] R. F. Stengel: "Optimal Control and Estimation", Dover Publications, (1994).
[11] A. Elcrat, B. Fornberg, M. Horn and K. Miller: "Some steady vortex flows past a circular cylinder", J. Fluid Mech. **409**, 13-27, (2000).
[12] V. S. Sadovskii: "Vortex regions in a potential stream with a jump of Bernoulli's constant at the boundary", Appl. Math. Mech. **35**, 729, (1971).
[13] M. .V. Melander, N. J. Zabusky and A. .M. Styczek: "A moment model for vortex interactions of two–dimensional Euler equations. Part 1 — Computational validation of a Hamiltonian elliptical representation", J. Fluid Mech. **167**, 95-115, (1986).
[14] B. Protas: "Higher–order Föppl models of steady wake flows", Phys. Fluids **18**, 117109, (2006).
[15] B. Protas: "Center Manifold Analysis of a Point–Vortex Model of Vortex Shedding with Control", (submitted), 2006.